Freeze/Thaw Detection and Validation Using Aquarius' L-Band Backscattering Data

Xiaolan Xu, *Member, IEEE*, Chris Derksen, Simon H. Yueh, *Fellow, IEEE*, Roy Scott Dunbar, and Andreas Colliander, *Senior Member, IEEE*

***Abstract*—The seasonal cycle of landscape freeze/thaw (FT) state across mid- to high latitudes influences critical processes such as the land surface energy balance, carbon cycle dynamics related to vegetation growth, and hydrological partitioning between surface runoff and infiltration. In this paper, we produce the first daily FT classification for the 2011–2014 period based on L-band radar measurements from Aquarius. The radar FT algorithm used in this paper is based on a seasonal threshold approach, which is also the baseline algorithm applied to higher-resolution (3 km) radar measurements from NASA's Soil Moisture Active/Passive (SMAP) mission (Launched January 31, 2015). The lower frequency (L-band) radar backscatter measurements from Aquarius provide enhanced sensitivity to FT conditions in vegetation canopy, snow and surface soil layers, although the relative radar penetration depth and sensitivity of the FT signal to these landscape elements will vary according to surface moisture and vegetation biomass conditions, and underlying land cover and terrain heterogeneity [1], [2]. Evaluation of the seasonal threshold FT algorithm using Aquarius was performed using surface air and soil temperatures from selected stations in the Snow Telemetry (SnoTel) network. Analysis identified good agreement during the fall freeze-up period with flag agreement exceeding the 80% SMAP accuracy target when summarized on a monthly basis. Disagreement was greater during the spring thaw transition due in part to uncertainty in characterizing thaw from *in situ* measurements. Unlike the fall season, stronger agreement in the spring was identified when the reference state was characterized with air temperature compared to soil temperature.**

***Index Terms*—Environmental monitoring, land surface, radar remote sensing.**

I. Introduction

OVER one-third of the global land area undergoes a seasonal transition between predominantly frozen and non-frozen conditions each year, with the land surface freeze/thaw (FT) state a significant control on hydrological and biospheric processes over northern land areas and at high elevations [3]. This transition is closely linked to the timing and length of the vegetation growing season [4], [5], the seasonal evolution of land–atmosphere carbon dioxide exchange [6]–[8], and interactions between soil processes and snow melt [9]. The land surface FT state is difficult to monitor with conventional observations due to sparse networks (particularly at high latitudes) and challenges related to the measurement of soil temperature. Unlike standard measurements such as air temperature, soil temperature is not monitored at all climate networks, measurement uncertainty is high if soil temperature probes are not calibrated site-specifically, and the vertical resolution of measurement profiles is not standard between networks.

Soil temperature information is available from modern reanalysis and data assimilation systems, but there is relatively high uncertainty between the land surface variables in these products [10] because of a lack of observations, relatively simplistic soil modeling schemes, and uncertainty in the treatment of soil processes (including layering, consideration of organic soils, etc. [11], [12]). Uncertainty in model products becomes especially significant when temperatures are close to the FT transition. Small biases of only 1° or 2° can result in the incorrect soil state.

Microwave remote sensing can provide terrestrial FT state information because of microwave sensitivity to surface permittivity, which is predominantly influenced by the phase of water. Both passive and active measurements at various frequencies and spatial resolutions have been applied to algorithms of varying levels of complexity.

There is a long time series of satellite passive microwave measurements, which have been exploited to produce an FT climate data record for the Northern Hemisphere based on a seasonal threshold-based temporal change classification [3], [13]. While providing daily coverage of land areas north of 45°N, passive microwave products are at a modest spatial resolution (25 km) and based on frequencies (Ku- and Ka-band) that are strongly influenced at certain times of the year by variables such as vegetation, snow cover, and the atmosphere. Despite these challenges, the long passive microwave satellite data record allows the determination of climate relevant trends in variables like melt onset date [14].

Scatterometer and SAR data have been utilized for FT retrieval with the active nature of these measurements providing a much improved spatial resolution (i.e., ~5 km for Ku-band QuikScat; ~12.5 km for C-band ASCAT onboard MetOp (High res mode); ~1 km for C-band ASAR on ENVISAT;) than the passive microwave time series. Regional studies at Ku- and C-band have shown a strong response to thaw onset in the spring over parts of Siberia by exploiting the diurnal differences between ascending and descending QuikScat orbits [15] and by

Manuscript received March 26, 2015; revised January 07, 2016; accepted January 08, 2016. Date of publication February 17, 2016; date of current version March 11, 2016. This work was supported by the Jet Propulsion Laboratory, California Institute of Technology, under a contract with the National Aeronautics and Space Administration. The Group for Level 2 Aquarius backscattering data were obtained from the NASA EOSDIS Physical Oceanography Distributed Active Archive Center (PO.DAAC) at the Jet Propulsion Laboratory, Pasadena, CA.

X. Xu, S. H. Yueh, R. S. Dunbar, and A. Colliander are with the Jet Propulsion Laboratory, California Institute of Technology, Pasadena, CA 91125 USA (e-mail: xiaolan.xu@jpl.nasa.gov).

C. Derksen is with the Environment Canada, Canada.

Color versions of one or more of the figures in this paper are available online at http://ieeexplore.ieee.org.

Digital Object Identifier 10.1109/JSTARS.2016.2519347

1939-1404 © 2016 IEEE. Personal use is permitted, but republication/redistribution requires IEEE permission.
See http://www.ieee.org/publications_standards/publications/rights/index.html for more information.

Authorized licensed use limited to: University of North Texas. Downloaded on December 18,2020 at 12:50:04 UTC from IEEE Xplore. Restrictions apply.

applying a temporal edge detection to time series of ASAR data [16]. A seasonal threshold approach was applied to QuikScat data over Alaska to determine freeze and thaw timing [17]. Daily pan-Arctic FT transitions (over both land and sea ice) were successfully derived from QuikScat data using an optimal edge detection scheme [18]. There are notable benefits to combining multiple measurement frequencies including improved temporal coverage. More elaborate data fusion techniques [19] are required to exploit the frequency dependent sensitivity to different elements of the surface including vegetation, snow, and soil properties [20].

To reduce sensitivity to vegetation, and maximize penetration depth under diverse imaging conditions, lower frequency microwave measurements at L-band are required. Recent work has illustrated the sensitivity of L-band radiometer measurements at the plot scale to seasonal dynamics of FT [21], although scaling challenges remain when utilizing spaceborne measurements from sensors like the Soil Moisture Ocean Salinity (SMOS) mission ($\sim$45-km spatial resolution [22]). High resolution L-band radar measurements from PALSAR have been utilized to effectively show local scale variability in FT transitions [1], [2]; however, the narrow swath of L-band SAR systems means the required coverage for synoptically sensitive hemispheric datasets is not available. Therefore, it is essential to develop an FT product from measurements at L-band frequency, with a moderate resolution to resolve some degree of landscape heterogeneity (i.e., 1–3 km), combined with a wide swath ($\sim$1000 km) to ensure daily coverage of northern regions during the important transitional seasons. Measurements with these characteristics are available for spring of 2015 from the NASA Soil Moisture Active Passive (SMAP) mission.

The SMAP FT product (L3_FT_A) provides a categorical (frozen, thawed, or [inverse] transitional) classification of the surface state for land areas north of 45° N. The SMAP algorithm is based on a seasonal threshold approach, which classifies the land surface FT state based on a well-established relationship between the time series of radar backscatter response and the change in dielectric constant of the land surface components associated with water transitioning between solid and liquid phases [1], [3], [23], [24]. The performance of the algorithm is highly dependent on the reference freeze and thaw backscatter values which must be pre-established on a pergrid cell basis, and the definition of a local (pergrid cell) threshold value used to determine whether daily backscatter measurements are classified as frozen or thawed.

Between 2011 and 2015, the Aquarius satellite acquired similar L-band backscatter measurements as SMAP, although at coarse spatial and temporal resolutions. The objectives of this study are to utilize the Aquarius dataset as a test bed to evaluate L-band radar response to FT transitions and establish and optimize the reference and threshold values for at-launch application to the SMAP FT product.

While still locally significant for ecological and agricultural impacts, climatologically, freeze events tend to be ephemeral south of approximately 45°N (particularly in nonalpine regions). The relative influence of FT and nonfrozen season effects on vegetation growth is less widespread at lower latitudes due to a general reduction of cold temperature constraints to productivity and a relative increase in other environmental controls such as moisture limitations [4]. Moreover, the threshold method used in this paper relies on a strong difference between the freeze and thaw reference. Reference value differences below approximately 1.5 dB will limit the ability to distinguish frozen versus thawed ground from the radar signal and significantly increase FT retrieval uncertainty. In those cases, additional ancillary data need to be included and more advanced data fusion techniques [19] are beneficial. In this study, our analysis with Aquarius data was limited to north of 45°N, consistent with the SMAP FT domain.

The outline of this paper is as follows. Section II will demonstrate the processing of the active backscatter measurements from the Aquarius L-band Level 2 product and the derivation of FT state using *in situ* measurements from reference stations. In Section III, we will review the implementation of the FT baseline algorithm. In Section IV, the validation will be performed by comparing FT retrievals with the *in situ* measurements and the overall retrieval performance will be analyzed. Finally, the discussion and conclusion will be given in Section V.

II. Data

A. Satellite Data

Aquarius is a combined active and passive L-band microwave instrument with the mission objectives to map the salinity field at the surface of the ocean from space and support studies of the coupling between ocean circulation, the global water cycle, and climate system. Aquarius radar measurements over land provide the first L-band backscatter dataset with global coverage coupled with a temporal revisit of one week, which is beneficial for the study of synoptically sensitive variables such as soil moisture [25] and landscape FT. The satellite was launched in June 2011, with data acquired since August 28, 2011. Aquarius ceased operation on June 7, 2015. The Aquarius antenna is a 2.5-m offset parabolic reflector with three horns, providing three beams with local incidence angles at 28.7°, 37.8°, and 45.6°. The resolution for the three beams is 76×94, 84×120, 96×156 km and collectively have a swath width of approximately 390 km. The active scatterometer is operated at 1.4 GHz. The observatory is in a sun-synchronous orbit with equatorial crossing times of 6 AM (descending) and 6 PM (ascending). The orbit is a 7-day exact repeat.

The gridded backscatter data used in this study are generated from Aquarius Level 2 version 3.0 dataset. Dual polarization measurements (vertical and horizontal) allow for four channels (vv hh hv vh) of backscattering coefficients. For seamless transition to the SMAP mission, we adopt the 36-km EASE Grid 2.0 [26], [27]. After regridding, each Aquarius footprint covers between 6- and 12- EASE grid cells. The ascending and descending orbits are processed separately for the three beams. Global coverage is achieved by taking a 7-day moving average and normalizing the three beam data to a 40° incidence angle. Therefore, the gridded backscatter dataset has daily global coverage. Radio frequency interference (RFI) was eliminated using the standard Aquarius flag.

Authorized licensed use limited to: University of North Texas. Downloaded on December 18,2020 at 12:50:04 UTC from IEEE Xplore. Restrictions apply.

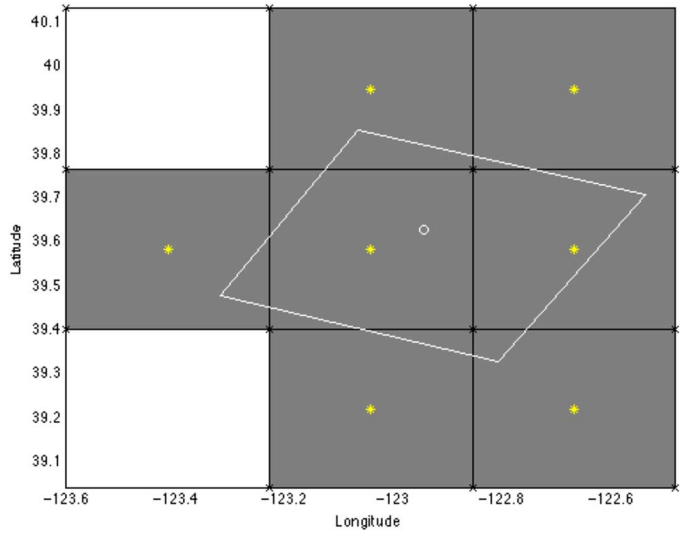

Fig. 1. White polygon is defined from the Aquarius 3-dB footprint corners. The white circle is the beam center. The yellow asterisks are the center of the EASE2 grid cells. The gray grids share some overlapping area with the Aquarius footprint.

The swath data in each beam are separately converted to the 3-km EASE Grid by averaging the data using the inverse distance weight (1) for each day. In Aquarius Level 2 products, the navigation group provides the beam center latitude/longitude along with the coordinates of the four footprint corners for the 3-dB scatterometer footprint [28]. Instead of using the actual oval-shape footprint, we approximate the footprint as quadrilateral. In Fig. 1, we show an example of a single Aquarius footprint over the EASE2 36-km global grid (M36). In this example, the backscatter (in natural unit) of this footprint will be assigned to the seven gray grids using inverse distance weighting. The distance is the geodesic arc length between the beam center and grid center assuming that the points lie on the WGS-84 ellipsoid. Each grid may be visited by several footprints in which case the assemble average is taken as

$$X_{IDW} = \frac{\sum_{i=1}^{N} X_i/(d_i)^p}{\sum_{i=1}^{N} 1/(d_i)^p} \tag{1}$$

d_i is the distance between the EASE2 grid center and Aquarius footprint center. X_i is the swath data (backscattering σ_0) and $p = 2$.

For each beam, we calculated the mean backscatter for each land cover type based on the International Geosphere Biosphere Project (IGBP) land cover classes as determined from MODIS imagery [29]. The incidence angle dependence slopes (dB per degree) were calculated for the 16 IGBP land cover classes using linear interpolation (Fig. 2). The slope coefficients were calculated over each 7-day moving window and updated over time. In Fig. 3, we show a 2-year time-series of the slope (dB/degree) change over the 16 IGBP classes. A clear seasonal cycle for needle leaf forest is evident because of incidence angle sensitivity to seasonal changes in the orientation and structure of the canopy (the coniferous canopy tends to be more vertical in winter). In the IGBP classification, most of the broadleaf forests are rainforests located close to the equator. The forest structure is fairly stable and the slope variability tends to be small (Fig. 3). Similarly, the open shrubland, savannas, grassland, and barren areas do not experience significant structure change over the season and also have stable slopes overtime. The slope fluctuation for cropland generally responds to changes in vegetation growth during the agricultural growing season. We applied the slopes and offsets for each land cover type to bin the three-beam Aquarius data to 40° to achieve global coverage at approximately the same incidence angle as SMAP. This set of processed gridded Aquarius data were utilized for all the following analysis. Because the daily global backscattering data consist of measurements extending over a week and include errors from incidence angle correction, swath-like artifacts in some places are visible; however, the FT seasonal threshold algorithm is grid independent so this does not introduce any extra error to the FT retrieval.

B. In Situ Reference Data

Land surface variables like soil moisture are measured directly at the surface, and so satellite retrieval validation is complicated primarily by spatial scaling issues. The validation of FT, however, is indirect because binary FT state is not directly measured but must be inferred from various temperature measurements. Instead, various measurements including air and soil temperature, soil moisture, snow depth and state (wet/dry), and vegetation temperature all influence the surface permittivity, which is controlling the radar response [10]. In order to understand the physical drivers behind seasonal transitions in the radar signal, comprehensive measurements of the vertical continuum of soil, snow, air, and vegetation are required, but are rarely available, if at all.

In this study, we validate the FT retrieval algorithm using *in situ* measurements from Snow Telemetry (SnoTel) network. The spatial distribution of the stations is shown in Fig. 4. To match the 100-km resolution of the Aquarius data, we chose stations located in the dominant land cover grid (green symbols in Fig. 4) to ensure the *in situ* measurements from the single

Authorized licensed use limited to: University of North Texas. Downloaded on December 18,2020 at 12:50:04 UTC from IEEE Xplore. Restrictions apply.

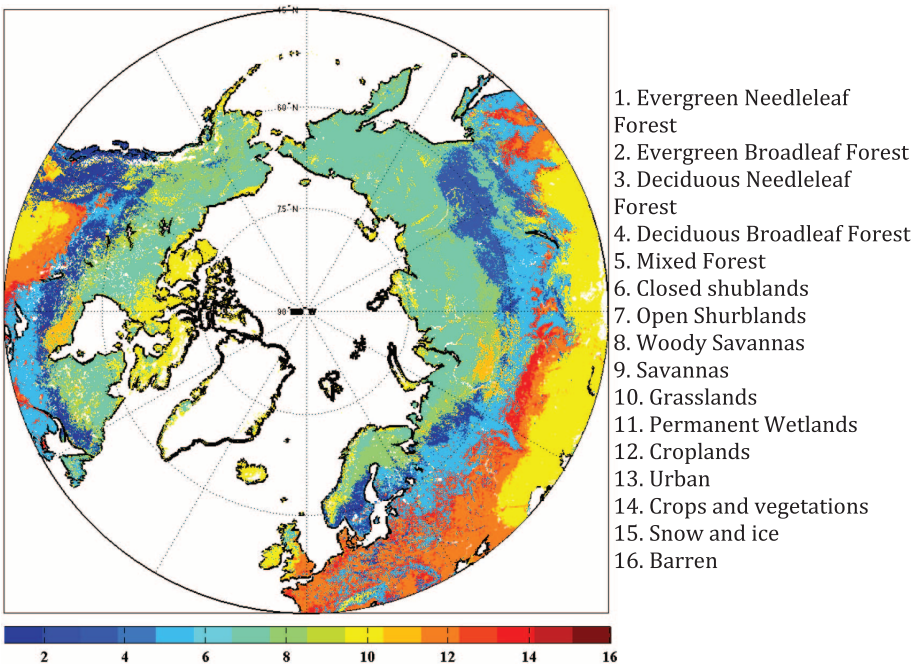

Fig. 2. MODIS derived 16 class IGBP land cover in the polar EASE2 grid.

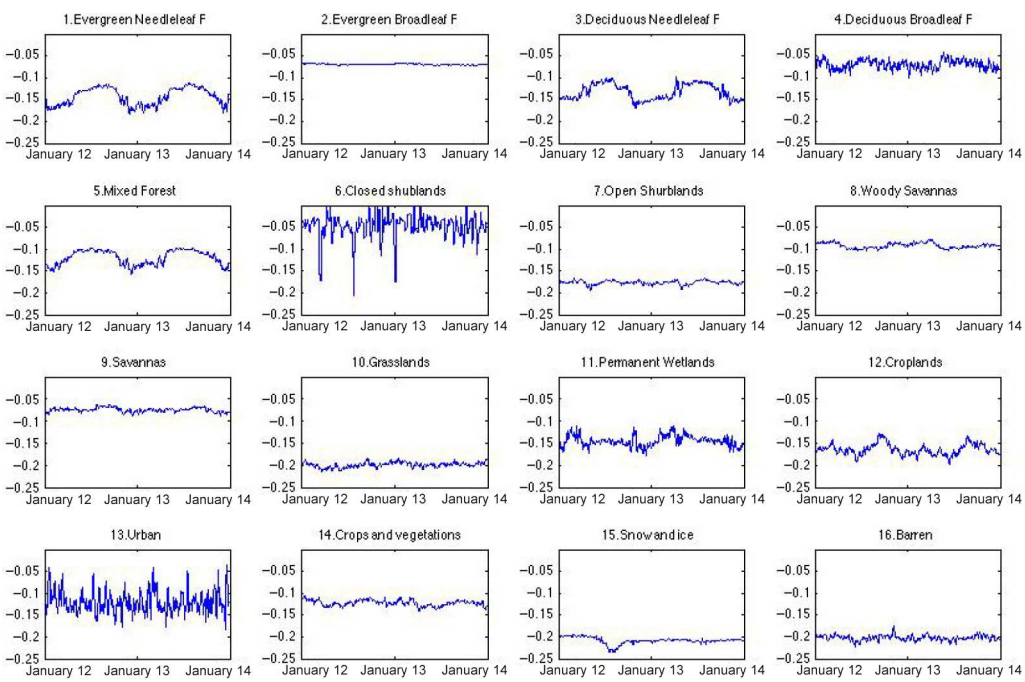

Fig. 3. Slope (dB/degree) coefficients for different land cover classes, calculated daily over each 7-day moving window in 2012–2014.

station represent the whole grid. We only used enhanced stations from the Natural Resources Conservation Service, which also include soil moisture and soil temperature measurements at 5-cm depth, along with 2-m air temperature and snow measurements. Only sites north of 45°N were retained consistent with the latitudinal extent of the SMAP FT product.

As noted earlier, there is ambiguity in how the binary landscape FT state is characterized using *in situ* measurements. We selected air temperature and soil temperature indicators of the FT status in order to investigate sensitivity of the validation process to how FT is characterized. Near-surface soil temperature directly captures the thermal state of the soil layer to which L-band backscatter measurements are theoretically sensitive, and provides the most straightforward physical connection between a single *in situ* variable and radar response. While air temperature is a commonly measured variable, it is unsatisfying for FT validation because it is only indirectly related to backscatter. In the presence of snow however, air temperature is a meaningful proxy for wet versus dry snow, which should have a strong effect on measured

Authorized licensed use limited to: University of North Texas. Downloaded on December 18,2020 at 12:50:04 UTC from IEEE Xplore. Restrictions apply.

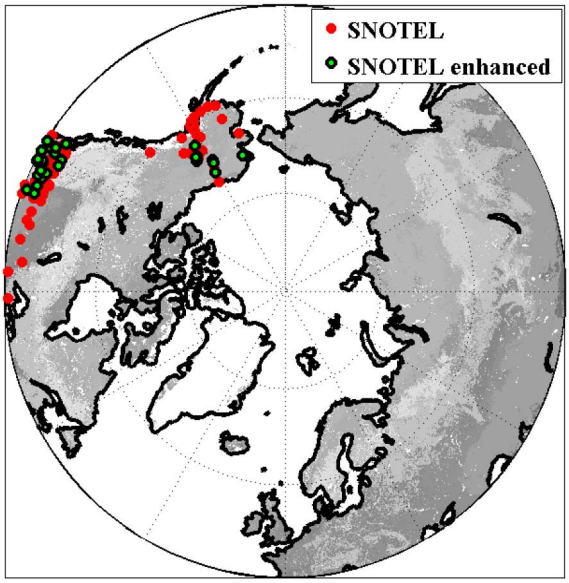

Fig. 4. *In situ* measurement stations in the SNOTEL network north of the 45°N. Green symbols denote stations retained for validation based on representativeness of the site land cover at the Aquarius resolution.

L-band backscatter (there is a general absence of systematic snow temperature measurements in any monitoring network). A threshold value of 0 °C was used to determine FT state from both soil and air temperature measurements. Hourly data are available from all selected stations in SnoTel network; to match with the daily ascending and descending backscatter, we average the hourly measurements into AM (1:00–12:00) and PM (13:00–24:00).

III. F Baseline Algorithm

The radar FT detection algorithm described here is based on a seasonal threshold approach, which is also applied to higher-resolution (3 km) L-band radar measurements from NASA's SMAP mission. The algorithm was previously developed and applied using time-series satellite remote sensing radar backscatter and radiometric brightness temperature data from a variety of sensors and frequencies [1], [23], [30]–[32]. When the soil status changes between frozen and thawed, the dielectric constant of the soil will change sharply. The characteristic of the soil emission and backscattering will also change and thus provide an opportunity for detecting the FT transition. Previous studies have demonstrated the FT transition from Ku- and Ka-band data (both active and passive; [3], [14], [18], [33]). However, these relatively higher frequencies have a higher optical depth, which reduces penetration through dense vegetation and snow. The longer wavelength at L-band exhibits reduced backscattering sensitivity to vegetation and snow. In the seasonal threshold approach, a scale factor $\Delta(t)$ is defined for an observation acquired at time t as

$$\Delta(t) = \frac{\sigma(t) - \sigma_{freeze}}{\sigma_{thaw} - \sigma_{freeze}} \tag{2}$$

where $\Delta(t)$ is the radar measurement acquired at time t, for which an FT classification is sought, and σ_{freeze} and σ_{thaw} are backscatter measurements corresponding to frozen and thawed reference states, respectively. A threshold level T (which has a typical default value of 0.5, but can be optimized) defines the thawed and frozen landscape states, respectively,

$$\Delta(t) > T$$
$$\Delta(t) < T. \tag{3}$$

To implement this algorithm, the freeze reference, thaw reference, and threshold need to be derived a priori. Two techniques are tested here for isolating reference states characteristic of frozen and thawed conditions. The first is a simple temporal average over January/February for freeze and July/August for thaw. The second approach averages a fixed number of the lowest (freeze) and highest (thaw) ranked seasonal backscatter values. In Fig. 5, we use references from 2012 as an example, and compare the difference of the thaw and freeze ($\sigma_{thaw} - \sigma_{freeze}$) from these two methods. Using the 10 lowest/highest ranked values provides a greater difference between the freeze and thaw states than the simple 2-month temporal average, thereby providing an overall stronger signal for FT distinction using the seasonal threshold method. In particular, the reference difference using the ranked average provides greater signal near the southern margin of the domain in western Eurasia. When the difference between the thaw reference and freeze reference is smaller than 2 dB (see Fig. 5), it means the soil permittivity does not change sufficiently because either the area is too dry or never goes through a seasonal FT cycle. Grid cells below the 2-dB threshold are flagged out.

The standard deviation of each grid for the 10 lowest-ranked backscattering values (Fig. 6) is very low for the freeze reference (generally < 0.3 dB), indicating a stable and consistent Aquarius derived reference. Regions of greater variability are evident for the thaw reference, likely due to summer season variability in vegetation water content (VWC). In Fig. 7, we plot the mean and standard deviation of the difference between the thaw and freeze reference for different land cover categories over the 2012–2014 period. In these 3 years, the difference between references stays fairly stable within each land cover type. Because the mean and standard deviation were calculated only for grid cells north of the N45, the evergreen broadleaf forest, deciduous broadleaf forest and urban classes contain too small a sample to determine robust statistics. The permanent ice and snow areas are flagged out. A larger mean difference and smaller standard deviation means a consistently good separation between the freeze and thaw states. These results show a relatively weak signal in grassland, cropland, and barren areas. Most of the grassland and cropland areas located north of N45 are actually very close to the southern latitudinal cutoff, and so are characterized by ephemeral FT cycles. Low vegetation areas, including those at high latitudes can be very dry in the summer, which makes the reference difference relatively low.

Spatial gaps due to radio frequency interference (RFI) in the Aquarius derived references can be filled by applying land cover specific averages to grid cells with missing values. In this study, the threshold (T) is fixed at 0.5. The threshold can be optimized during the transition seasons using air or soil temperature data from reanalysis (as applied by [1]) and will be addressed in future work).

Authorized licensed use limited to: University of North Texas. Downloaded on December 18,2020 at 12:50:04 UTC from IEEE Xplore. Restrictions apply.

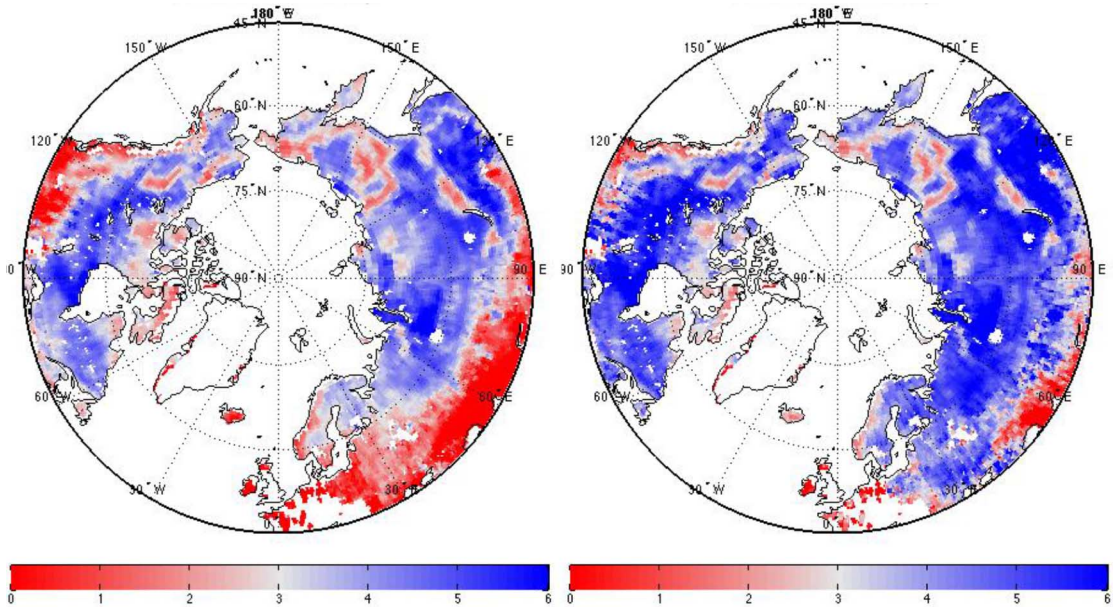

Fig. 5. For 2012, difference in σ_{thaw} and σ_{freeze} references derived from: (a) averaging over two months (January/February and July/August), and (b) 10 highest and lowest backscatter values from the same months.

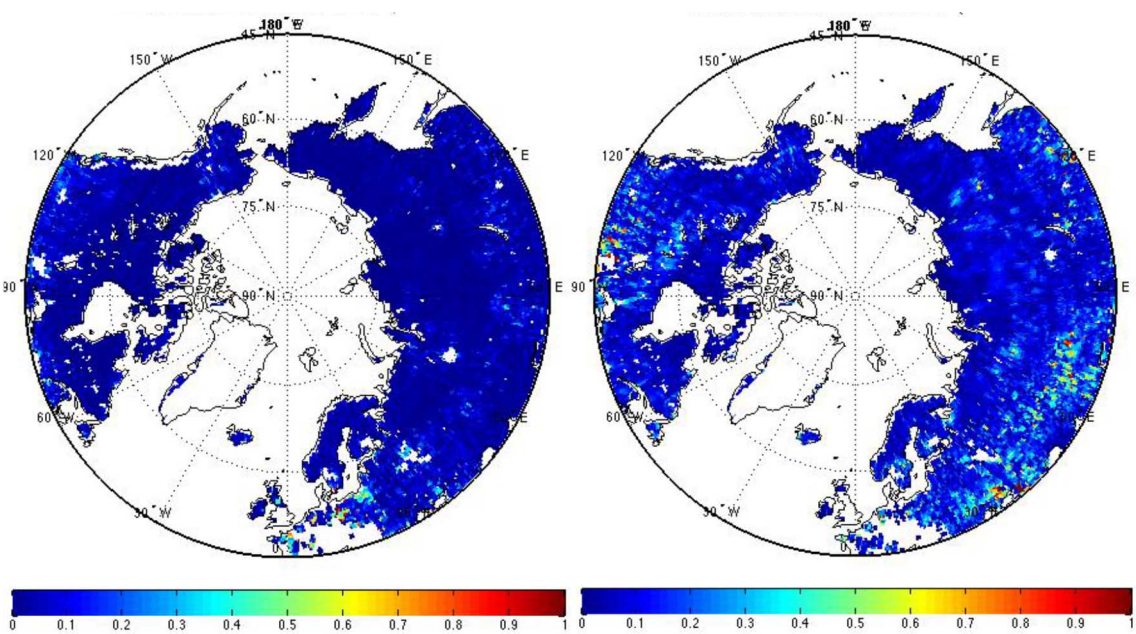

Fig. 6. For 2012: (a) freeze reference standard deviation and (b) thaw reference standard deviation.

IV. Validation and Analysis

Evaluation of the FT algorithm based on Aquarius data was performed using reference measurements from selected stations in the SnoTel network. We followed the validation framework developed for the SMAP mission and define the following parameter to access the retrieval accuracy.

Let $A(i,t)$ denote the Aquarius-retrieved FT flag at time t and over validation area i. The index for validation area i correspond to an independent ground-truth observation that is located within the grid, referred as a "validation observation." Let $\mathrm{v}(\mathrm{i},\mathrm{t})$ denotes the corresponding independent ground-truth observation. For the networks used in this study, a validation observation will be an individual *in situ* sensor location (note that a limited number of spatially intensive *in situ* sites will also be included in SMAP FT cal/val). The time span covered by the paired observations is chosen to cover the desired duration for evaluating the mean level of agreement.

The computation of the classification accuracy proceeds as follows: let $\mathrm{A}_{\mathrm{AM/PM}}(\mathrm{i},\mathrm{t}) = 1$ if the Aquarius retrieved flag at grid cell i (on the SMAP 36 km EASE grid) and time t indicates frozen conditions for AM (descending) or PM (ascending) overpass, respectively, and let $\mathrm{A}_{\mathrm{AM/PM}}(\mathrm{i},\mathrm{t}) = 0$ if the Aquarius retrieved flag indicates thawed conditions for AM or PM overpass, respectively. Likewise, let $\mathrm{v}_{\mathrm{AM/PM}}(\mathrm{i},\mathrm{t}) = 1$ if the

Authorized licensed use limited to: University of North Texas. Downloaded on December 18,2020 at 12:50:04 UTC from IEEE Xplore. Restrictions apply.

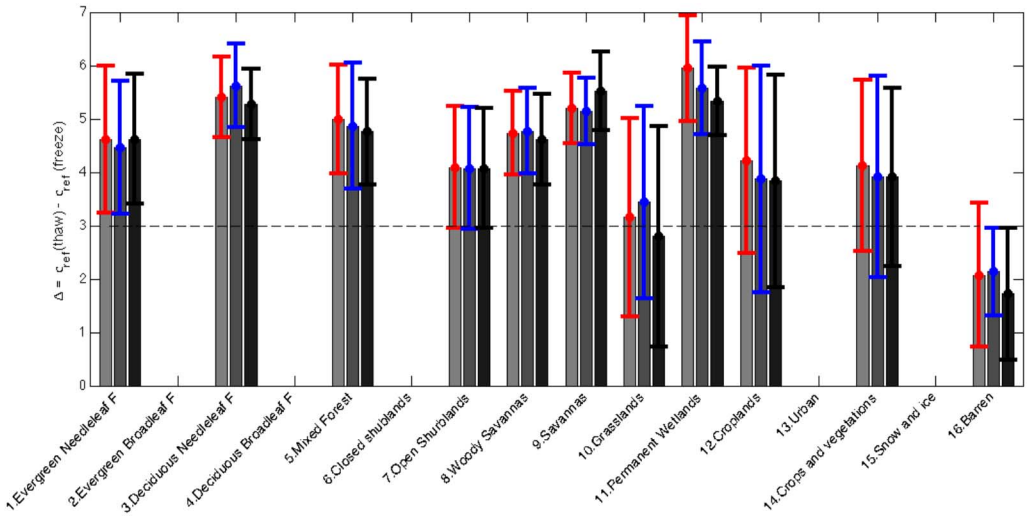

Fig. 7. Mean and standard deviation of the FT reference difference by IGBP land cover class.

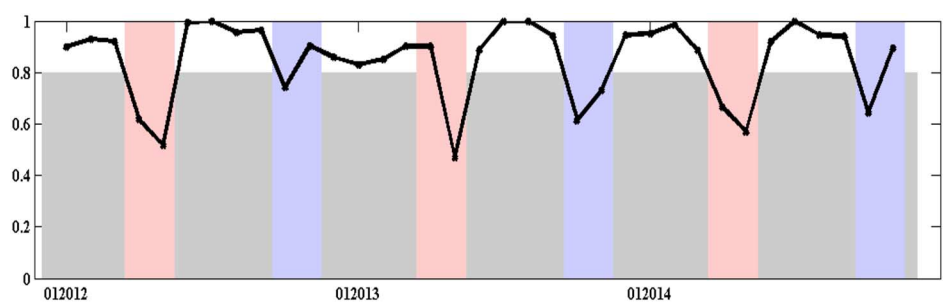

Fig. 8. Overall FT retrieval performance for SNOTEL stations in 2012–2014. The red areas denote March 15–May 15 each year and the blue areas denote September 15–November 15.

corresponding reference flag indicates frozen conditions at the AM or PM overpass and $\mathrm{v_{AM/PM}(i,t)} = 0$ for thawed conditions at the AM or PM overpass. Next, the error flag δ is set by comparing the Aquarius FT retrievals to the validation observations

$$\delta_{AM,PM}(i,t) = \begin{cases} 0, \text{ if } A_{AM,PM}(i,t) = v_{AM,PM}(i,t) \\ 1, \text{ if } A_{AM,PM}(i,t) \neq v_{AM,PM}(i,t). \end{cases} \tag{4}$$

Note that a single AQ-retrieved flag is produced each day, but is derived from separate descending (AM) and ascending (PM) overpasses. The Aquarius-retrieved flags will therefore be separated back into binary FT classes for the AM and PM orbits, producing two retrieval match-ups each day.

We define a target accuracy of 80% flag agreement (consistent with the SMAP mission requirement)

$$1 - \sum\nolimits_i^{N_i} \sum\nolimits_t^{N_t(i)} \delta(i,t) / \sum\nolimits_t^{N_i} N_t(i) \geq 0.8. \tag{5}$$

Equation (5) can solved using various temporal aggregations of measurements, thereby providing an instantaneous (e.g., daily) determination of FT spatial accuracy across the available reference sites, or a metric of performance over longer time periods (i.e., months, seasons, and years). In this study, retrieval performance will be summarized monthly to reduce sensitivity to prolonged periods of consistent frozen and thawed states in the winter and summer, respectively.

In Fig. 8, we show the overall performance in 2012–2014 of the FT algorithm over the reference network. The red areas are marked March 15–May 15 to indicate the freeze to thaw transition period while blue areas are marked from September 15 to November 15 to indicate the thaw to freeze transition. The SNOTEL network has a relatively high number of stations in Alaska. The accuracy stays above 80% for most of the months. The challenge posed by the freeze to thaw transition is also evident with the SnoTel sites. Because they are predominantly in Alaska, agreement is high ($< 85\%$) from January through March during stable freeze conditions. Flag agreement decreases during the transition months of April and May. Scaling challenges no doubt influence these results. Using single point soil temperature measurements for validation of a spatially integrated satellite FT retrieval is always imperfect due to heterogeneity introduced by land cover, slope, aspect, vegetation, and snow distribution. This issue is evident with high resolution PALSAR data [1], [2] and so will be greatly exacerbated at the extremely coarse resolution of the Aquarius measurements.

In Fig. 9, a time series plot for an example SnoTel station in Alaska is shown over 2012–2014. The two thick dashed black lines indicate the freeze and thaw references; the dashed gray

Authorized licensed use limited to: University of North Texas. Downloaded on December 18,2020 at 12:50:04 UTC from IEEE Xplore. Restrictions apply.

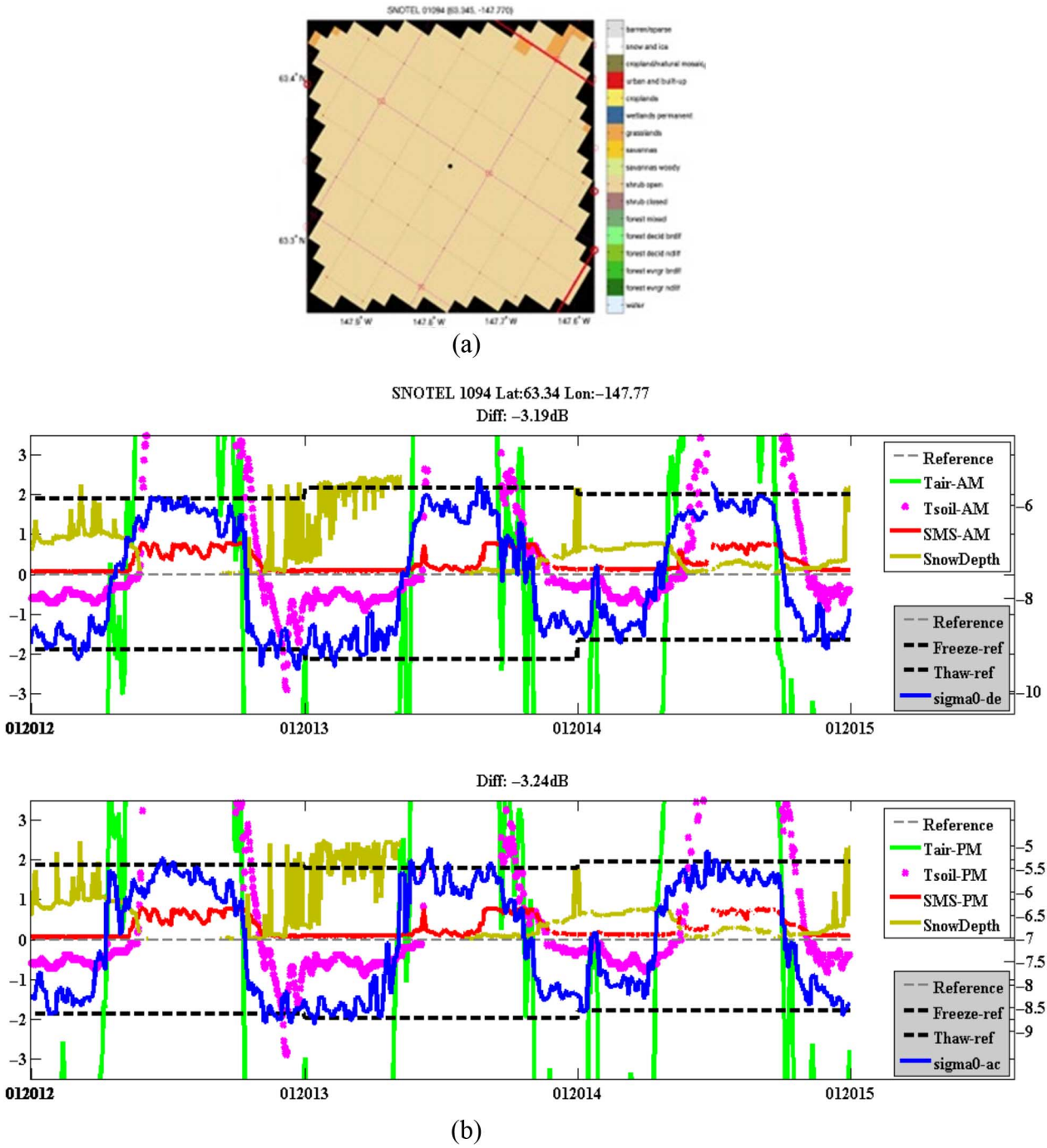

Fig. 9. (a) Monahan Flat SnoTel site in the EASE2 grid. (b) Example Aquarius backscatter time series with *in situ* measurements from Monahan Flat SNOTEL site, 2012–2014, ascending pass. The back dashed line is the FT reference (scale on right axis). The blue line is the backscattering signal with the gray dash line as the 0.5-threshold. The *in situ* SNOTEL measurements read to the left axis with light green as the air temperature in Celsius, magenta as soil temperature in Celsius, red as soil moisture in volumetric percentage, and yellow as snow depth in meter.

line is the 0.5-threshold. The blue line is the backscattering indicator $\Delta(t)$, which above the 0.5-threshold identifies a frozen flag and below indicates thaw. The air/soil temperature reads on the left axis in Celsius limited to $\pm 3°$ to provide sufficient detail during the transition period. Overall, the retrieved flags agree well with the primary freeze and thaw events but there are some key differences between seasons. During the freezing process, the air temperature, soil temperature, and Aquarius flags identify freezing at the same time in early November. During the thaw transition, however, the radar clearly responds to the onset of snowmelt consistent with air temperatures rising above zero. These conditions (wet snow; soil temperature below freezing) persist for 2–3 weeks and are typical of subarctic conditions during melt.

In Fig. 10, we compare the retrieved FT flag accuracy against the reference FT state determined from soil and air temperatures, respectively, for both ascending and descending passes over the SNOTEL sites. During the fall and winter seasons,

Authorized licensed use limited to: University of North Texas. Downloaded on December 18,2020 at 12:50:04 UTC from IEEE Xplore. Restrictions apply.

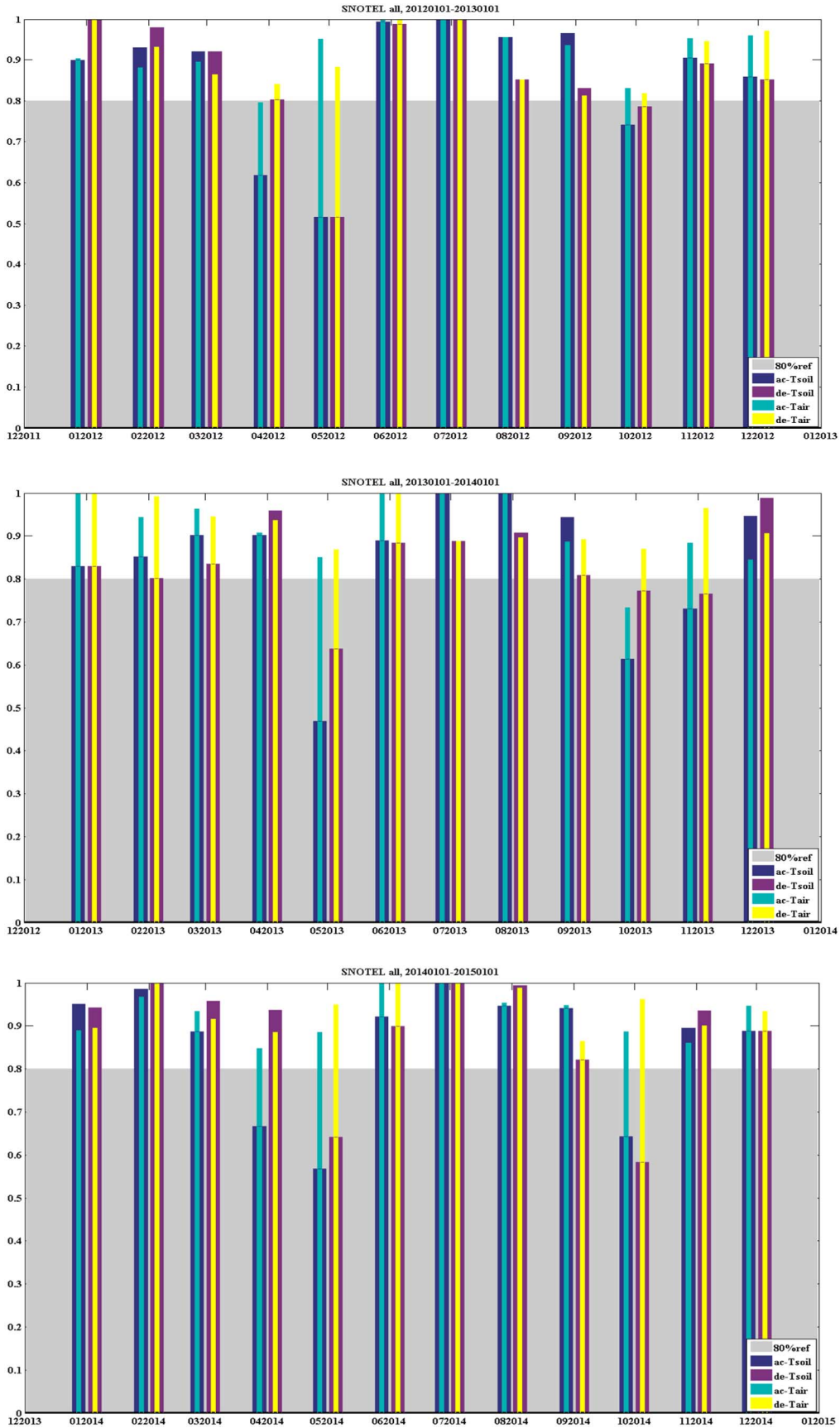

Fig. 10. Monthly FT flag agreement for all validated SnoTel sites, 2013–2014. Narrow columns indicate use of air temperature measurements for validation; wide columns indicate use of 5-cm soil temperature. Gray shading indicates 80% flag agreement requirement set by the SMAP mission.

Authorized licensed use limited to: University of North Texas. Downloaded on December 18,2020 at 12:50:04 UTC from IEEE Xplore. Restrictions apply.

TABLE I
MONTHLY AGREEMENT BETWEEN AQUARIUS AND REFERENCE FLAGS DERIVED AT SNOTEL STATIONS USING 5-CM SOIL TEMPERATURE

2014 SNOTEL versus AQUARIUS RETRIVED_AQ	Agree all	Error all	AQ = F Obs = F	AQ = T Obs = T	AQ = F Obs = T	AQ = T Obs = F
2014.01	0.95	0.05	0.95	0.00	0.00	0.05
2014.01	0.94	0.06	0.94	0.00	0.00	0.06
2014.02	0.98	0.02	0.98	0.00	0.00	0.02
2014.02	1.00	0.00	1.00	0.00	0.00	0.00
2014.03	0.89	0.11	0.80	0.09	0.00	0.11
2014.03	0.96	0.04	0.85	0.11	0.00	0.04
2014.04	0.67	0.33	0.49	0.18	0.00	0.33
2014.04	0.94	0.06	0.75	0.19	0.00	0.06
2014.05	0.57	0.43	0.02	0.55	0.00	0.43
2014.05	0.64	0.36	0.15	0.49	0.00	0.36
2014.06	0.92	0.08	0.00	0.92	0.00	0.08
2014.06	0.90	0.10	0.00	0.90	0.00	0.10
2014.07	1.00	0.00	0.00	1.00	0.00	0.00
2014.07	1.00	0.00	0.00	1.00	0.00	0.00
2014.08	0.95	0.05	0.00	0.95	0.05	0.00
2014.08	0.99	0.01	0.00	0.99	0.01	0.00
2014.09	0.94	0.06	0.03	0.92	0.02	0.04
2014.09	0.82	0.18	0.04	0.78	0.15	0.03
2014.10	0.64	0.36	0.34	0.30	0.31	0.04
2014.10	0.58	0.42	0.37	0.22	0.40	0.02
2014.11	0.89	0.11	0.82	0.08	0.05	0.05
2014.11	0.94	0.06	0.87	0.07	0.06	0.01
2014.12	0.89	0.11	0.79	0.09	0.11	0.00
2014.12	0.89	0.11	0.79	0.09	0.11	0.00
Overall	0.87	0.13	0.46	0.41	0.05	0.08

First line of each month is the ascending/PM pass and the second line is descending/AM pass.

the air temperature and soil temperature flags yield very similar performance metrics, which are above the 80% mission requirement threshold set for SMAP. This indicates freeze onset is coincident to air and soil temperature both falling below zero near concurrently. If snow is present at this time, it is typically dry. During spring, there can be a pronounced time lag between snowmelt onset and soil temperature response (as illustrated in Fig. 9). Due to the response of the radar to wet snow, the overall accuracy over the thaw transition is lower if soil temperature is used for deriving the *in situ* FT flag (Fig. 10). The stronger retrieval agreement with the air temperature flag indicates the radar is responding to wet snow.

A summary of the evaluation of the Aquarius derived FT product using observations from the SnoTel network is shown in Table I. The statistics were computed using 2014 data, for 12 stations (8 in Alaska; 4 in the northwest U.S.) and ascending/descending separately (the first row for each month is ascending/ PM overpass and the second row is descending/ AM). In this example, it is evident that the primary source of uncertainty in the Aquarius derived FT retrievals is during the thaw transition when the reference data indicate frozen ground and the radar retrieves a thawed state. Again, this is consistent with the influence of wet snow on the radar signal.

V. CONCLUSION AND DISCUSSION

In this paper, we apply a seasonal threshold algorithm to Aquarius L-band radar data to detect the FT status across northern hemisphere land areas north of 45°N. Different methods were tested to determine the freeze and thaw references. To better capture the upper and lower backscatter limit (and thereby increase the freeze versus thaw signal), we applied the average of the highest and lowest 10 backscatter values in July/August and January/February as the thaw and freeze references. The retrieved FT flags were validated against air temperature and soil temperature reference flags derived from stations in the SnoTel network. These freeze and thaw references derived from Aquarius data were implemented in the SMAP at-launch FT algorithm and will be cross compared with the SMAP FT product in the future.

This study has confirmed that despite the coarse spatial resolution, L-band radar measurements from Aquarius are sensitive to the FT state of the land surface. The landscape FT state retrieval, however, characterizes the predominant frozen or nonfrozen state of the land surface within a very large sensor field-of-view (FOV) and does not distinguish FT characteristics among different landscape elements, including surface snow, soil, open water, or vegetation. The lower frequency L-band measurements have greater sensitivity to surface soil FT conditions under low to moderate vegetation cover, but effective radar penetration depth and microwave FT sensitivity is still constrained by intervening vegetation biomass, soil moisture levels, and snow wetness. Ambiguity in relating changes in the radar signal to these specific landscape components is a challenge to validation of any FT product [10]. Introducing ancillary data such as global reanalysis temperature or snow cover flags (similar to ASCAT FT algorithm) will increase the accuracy in those areas. It will be investigated further in future research. In

Authorized licensed use limited to: University of North Texas. Downloaded on December 18,2020 at 12:50:04 UTC from IEEE Xplore. Restrictions apply.

northern boreal and tundra landscapes L-band penetration depth and soil sensitivity is greater under frozen conditions when land surface liquid water levels are low, and markedly reduced under thawed conditions due to characteristically moist surface organic layer and soil active layer conditions, even under relatively low tundra vegetation biomass levels [17].

The seasonal threshold FT classification algorithm employed in this study requires the establishment of accurate and stable frozen and nonfrozen reference backscatter values for each grid cell. The resulting spatial classification error is expected to be larger at lower latitudes (i.e., $\sim 45°\mathrm{N}$), where FT is ephemeral and the difference between frozen and thawed radar references is relatively small, and over complex terrain where FT heterogeneity is larger. The seasonal threshold algorithm also allows optimization of the threshold (T) value, which remained fixed in this study. Our results, however, provide guidance to future optimization of the threshold for L-band retrievals from radar or radiometer measurements. During the fall season, there is clear evidence the radar is responding to soil freeze, so surface soil layer temperature from reanalysis such as MERRA [30] would be most appropriate for threshold optimization. During spring, however, soil temperature would not be an appropriate variable: the strong response to wet snow makes air temperature more suitable.

A major assumption of the seasonal threshold based temporal dB change FT classification is that the major temporal shifts in radar backscatter are caused by land surface dielectric changes from temporal FT transitions. This assumption generally holds for higher latitudes and elevations where seasonal frozen temperatures are a significant part of the annual cycle and a large constraint to land surface water mobility and ecosystem processes. However, FT classification accuracy is expected to be reduced where other environmental factors may cause large temporal shifts in radar backscatter, including large rainfall events and surface inundation and abrupt changes in vegetation biomass (e.g., phenology, disturbance, and land cover change). Under relatively low land surface moisture levels, including arid and semi-arid zones, land surface dielectric changes and radar backscatter response to FT transitions is reduced, and may be a secondary dielectric response compared to other environmental changes including seasonal precipitation variations; the FT classification accuracy is expected to be reduced for these areas and conditions.

Acknowledgment

The authors would like to thank E. G. Njoku and J. Kimball for the valuable discussion and the reviewers for their helpful and insightful comments.

References

[1] E. Podest, K. C. McDonald, and J. S. Kimball, "Multisensor microwave sensitivity to freeze/thaw dynamics across a complex boreal landscape," *IEEE Trans. Geosci. Remote Sens.*, vol. 52, no. 11, pp. 6818–6828, Nov. 2014.

[2] J. Du, J. S. Kimball, M. Azarderakhsh, R. S. Dunbar, M. Moghaddam, and K. C. McDonald, "Classification of Alaska spring thaw characteristics using satellite L-band radar remote sensing," *IEEE Trans. Geosci. Remote Sens.*, vol. 53, no. 1, pp. 542–556, Jan. 2015.

[3] Y. Kim, J. S. Kimball, K. Zhang, and K. C. McDonald, "Satellite detection of increasing Northern Hemisphere non-frozen seasons from 1979 to 2008: Implications for regional vegetation growth," *Remote Sens. Environ.*, vol. 121, pp. 472–487, Jun. 2012.

[4] Y. Kim, J. Kimball, K. Zhang, K. Didan, I. Velicogna, and K. McDonald, "Attribution of divergent northern vegetation growth responses to lengthening non-frozen seasons using satellite optical-NIR and microwave remote sensing," *Int. J. Remote Sens.*, vol. 35, pp. 3700–3721, 2014.

[5] Y. Kim, J. Kimball, K. Didan, and G. Henebry, "Response of vegetation growth and productivity to spring climate indicators in the conterminous united states derived from satellite remote sensing data fusion," *Agric. For. Meteorol.*, vol. 194, pp. 132–143, 2014.

[6] M. Goulden *et al.*, "Sensitivity of boreal forest carbon balance to soil thaw," *Science*, vol. 279, pp. 214–217, 1998.

[7] T. Black *et al.*, "Increased carbon sequestration by a boreal deciduous forest in years with a warm spring," *Geophys. Res. Lett.*, vol. 27, pp. 1271–1274, 2000.

[8] K. C. McDonald, J. S. Kimball, E. Njoku, R. Zimmermann, and M. Zhao, "Variability in springtime thaw in the terrestrial high latitudes: Monitoring a major control on the biospheric assimilation of atmospheric CO_2 with spaceborne microwave remote sensing," *Earth Interact.*, vol. 8, pp. 1–23, 2004.

[9] A. C. Edwards, R. Scalenghe, and M. Freppaz, "Changes in the seasonal snow cover of alpine regions and its effect on soil processes: A review," *Quat. Int.*, vol. 162, pp. 172–181, 2007.

[10] L. Mudryk, P. Kushner, and C. Derksen, "Interpreting observed northern hemisphere snow trends with large ensembles of climate simulations," *Clim. Dyn.*, vol. 43, pp. 345–359, 2014.

[11] L. Farhadi, R. H. Reichle, G. J. M. De Lannoy, and J. S. Kimball, "Assimilation of freeze-thaw observations into the NASA catchment land surface model," *J. Hydrometeorol.*, vol. 16, pp. 730–743, Apr. 1, 2015.

[12] R. H. Reichle *et al.*, "Assessment and enhancement of MERRA land surface hydrology estimates," *J. Clim.*, vol. 24, pp. 6322–6338, Dec. 1, 2011.

[13] J. S. Kimball, K. C. McDonald, S. W. Running, and S. E. Frolking, "Satellite radar remote sensing of seasonal growing seasons for boreal and subalpine evergreen forests," *Remote Sens. Environ.*, vol. 90, pp. 243–258, 2004.

[14] L. Wang, C. Derksen, R. Brown, and T. Markus, "Recent changes in pan-Arctic melt onset from satellite passive microwave measurements," *Geophys. Res. Lett.*, vol. 40, pp. 522–528, 2013.

[15] A. Bartsch, R. A. Kidd, W. Wagner, and Z. Bartalis, "Temporal and spatial variability of the beginning and end of daily spring freeze/thaw cycles derived from scatterometer data," *Remote Sens. Environ.*, vol. 106, pp. 360–374, Feb. 15, 2007.

[16] S.-E. Park, A. Bartsch, D. Sabel, W. Wagner, V. Naeimi, and Y. Yamaguchi, "Monitoring freeze/thaw cycles using ENVISAT ASAR global mode," *Remote Sens. Environ.*, vol. 115, pp. 3457–3467, 2011.

[17] A. Colliander, K. McDonald, R. Zimmermann, R. Schroeder, J. S. Kimball, and E. G. Njoku, "Application of QuikSCAT backscatter to SMAP validation planning: Freeze/thaw state over ALECTRA sites in Alaska from 2000 to 2007," *IEEE Trans. Geosci. Remote Sens.*, vol. 50, no. 2, pp. 461–468, Feb. 2012.

[18] J. Mortin, T. M. Schrøder, A. W. Walløe Hansen, B. Holt, and K. C. McDonald, "Mapping of seasonal freeze-thaw transitions across the pan-Arctic land and sea ice domains with satellite radar," *J. Geophys. Res.*, vol. 117, C8, p. C08004, 2012.

[19] S. Zwieback, A. Bartsch, T. Melzer, and W. Wagner, "Probabilistic fusion of Ku- and C-band scatterometer data for determining the freeze/thaw state," *IEEE Trans. Geosci. Remote Sens.*, vol. 50, no. 7, pp. 2583–2594, Jul. 2012.

[20] S. M. Bateni, H. Chunlin, S. A. Margulis, E. Podest, and K. McDonald, "Feasibility of characterizing snowpack and the freeze–thaw state of underlying soil using multifrequency active/passive microwave data," *IEEE Trans. Geosci. Remote Sens.*, vol. 51, no. 7, pp. 4085–4102, Jul. 2013.

[21] K. Rautiainen *et al.*, "L-band radiometer observations of soil processes in boreal and subarctic environments," *IEEE Trans. Geosci. Remote Sens.*, vol. 50, no. 5, pp. 1483–1497, May 2012.

[22] K. Rautiainen *et al.*, "Detection of soil freezing from L-band passive microwave observations," *Remote Sens. Environ.*, vol. 147, pp. 206–218, 2014.

[23] E. Rignot and J. B. Way, "Monitoring freeze—Thaw cycles along north–south alaskan transects using ERS-1 SAR," *Remote Sens. Environ.*, vol. 49, pp. 131–137, 1994.

[24] J. S. Kimball, K. C. McDonald, A. R. Keyser, S. Frolking, and S. W. Running, "Application of the NASA scatterometer (NSCAT) for determining the daily frozen and nonfrozen landscape of Alaska," *Remote Sens. Environ.*, vol. 75, pp. 113–126, Jan. 2001.

Authorized licensed use limited to: University of North Texas. Downloaded on December 18,2020 at 12:50:04 UTC from IEEE Xplore. Restrictions apply.

[25] R. Bindlish, T. Jackson, M. Cosh, T. Zhao, and P. O'Neill, "Global soil moisture from the Aquarius/SAC-D satellite: Description and initial assessment," *IEEE Geosci. Remote Sens. Lett.*, vol. 12, no. 5, pp. 923–927, May 2015.

[26] M. Brodzik, B. Billingsley, T. Haran, B. Raup, and M. Savoie, "Correction: Brodzik, M. J., et al. EASE-Grid 2.0: Incremental but significant improvements for earth-gridded data sets. ISPRS International Journal of Geo-Information 2012, 1, 32-45," *ISPRS Int. J. Geo-Inf.*, vol. 3, pp. 1154–1156, 2014.

[27] M. J. Brodzik, B. Billingsley, T. Haran, B. Raup, and M. H. Savoie, "EASE-Grid 2.0: Incremental but significant improvements for earth-gridded data sets," *ISPRS Int. J. Geo-Inf.*, vol. 1, pp. 32–45, 2012.

[28] P. Jeffrey *et al.*, *Aquarius Radiometer Post-Launch Calibration for Product Version 2.0*, Aquarius Project Document: AQ-014-PS-0015 [Online]. Available: http://nsidc.org/data/aquarius/research.html

[29] C. Justice *et al.*, "An overview of MODIS land data processing and product status," *Remote Sens. Environ.*, vol. 83, pp. 3–15, 2002.

[30] J. Gamon *et al.*, "Remote sensing in BOREAS: Lessons learned," *Remote Sens. Environ.*, vol. 89, pp. 139–162, 2004.

[31] J. Way, R. Zimmermann, E. Rignot, K. McDonald, and R. Oren, "Winter and spring thaw as observed with imaging radar at BOREAS," *J. Geophys. Res.: Atmos.*, vol. 102, pp. 29673–29684, 1997.

[32] D. Entekhabi *et al.*, "The hydrosphere state (Hydros) satellite mission: An Earth system pathfinder for global mapping of soil moisture and land freeze/thaw," *IEEE Trans. Geosci. Remote Sens.*, vol. 42, no. 10, pp. 2184–2195, Oct. 2004.

[33] K. C. K. J. S. McDonald, "Estimation of surface freeze-thaw states using microwave sensors," in *Encyclopedia of Hydrological Sciences*. Hoboken, NJ, USA: Wiley, 2005.

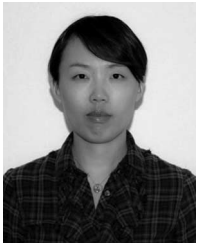

Xiaolan Xu (S'09–M'12) received the B.Eng. degree in electrical engineering from Zhejiang University, Hangzhou, China, in 2006, and the M.S. and Ph.D. degrees in electrical engineering from the University of Washington, Seattle, WA, USA, in 2008 and 2011, respectively.

In 2012, she was a Postdoctoral Research Associate with the Water and Carbon Cycles Group, Jet Propulsion Laboratory (JPL), California Institute of Technology, Pasadena, CA, USA, and a Scientist with Surface Hydrology Group of Earth Science Division since 2014. Her research interests include theoretical studies and numerical simulation in the random media scattering and its application in microwave remote sensing of terrestrial snow, soil properties, and vegetation biomass.

Chris Derksen received the B.E.S., M.A., and Ph.D. degrees in geography from the University of Waterloo, Waterloo, ON, Canada, in 1997, 1998, and 2001, respectively.

He has been a Research Scientist with the Climate Research Division of Environment Canada, ON, Canada, and holds an Adjunct Faculty Position with the Department of Geography and Environmental Management, University of Waterloo. His research interests include remote sensing of terrestrial snow cover, and the use of satellite derived datasets to identify interactions between the climate system and the cryosphere.

Simon H. Yueh (F'09) received the Ph.D. degree in electrical engineering in January 1991 from the Massachusetts Institute of Technology, Cambridge, MA, USA.

He was a Postdoctoral Research Associate with the Massachusetts Institute of Technology from February to August 1991. In September 1991, he was with the Radar Science and Engineering Section, Jet Propulsion Laboratory (JPL). From 2002 to 2007, He was the Supervisor with Radar System Engineering and Algorithm Development Group. He was the Deputy Manager of Climate, Oceans and Solid Earth Section from 2007 to 2009, and the Section Manager from 2009 to 2013. He was the Project Scientist with the National Aeronautics and Space Administration (NASA) Aquarius mission from January 2012 to September 2013, the Deputy Project Scientist with the NASA Soil Moisture Active Passive Mission from January 2013 to September 2013, and the SMAP Project Scientist since October 2013. He has been the Principal/Co-Investigator of numerous NASA and DOD research projects on remote sensing of soil moisture, terrestrial snow, ocean salinity, and ocean wind. He has authored four book chapters and published in more than 150 publications and presentations.

Dr. Yueh was an Associate Editor of IEEE TRANSACTIONS ON GEOSCIENCE AND REMOTE SENSING. He was the recipient of the IEEE GRSS Transaction Prize Paper Award in 1995, 2002, 2010, and 2014, the 2000 Best Paper Award in the IEEE International Geoscience and Remote Symposium, the JPL Lew Allen Award in 1998, and Ed Stone Award in 2003. He was also the recipient of the NASA Exceptional Technology Achievement Medal in 2014.

Roy Scott Dunbar received the B.S. in physics and astronomy from the University of Albany, Albany, NY, USA, in 1976, and the Ph.D. degree in physics from Princeton University, Princeton, NJ, USA, in 1980.

Since 1981, he has been with the Jet Propulsion Laboratory.

Andreas Colliander (S'04–A'06–M'07–SM'08) received the M.Sc. (Tech.), and D.Sc. (Tech.) degrees in electrical engineering from Helsinki University of Technology (TKK; now Aalto University), Espoo, Finland, in 2002 and 2007, respectively.

He has been a Research Scientist with the Surface Hydrology Group, Jet Propulsion Laboratory, California Institute of Technology, Pasadena, CA, USA. His research interests include utilization of microwave remote sensing to hydrological applications.

Dr. Colliander has been serving as a Co-Chair of the Microwave Radiometry Working Group of the Instrumentation and Future Technologies Technical Committee of the IEEE Geoscience and Remote Sensing Society since 2009. He is a Member of the Science Algorithm Development Team for the Soil Moisture Active and Passive (SMAP) mission.

Authorized licensed use limited to: University of North Texas. Downloaded on December 18,2020 at 12:50:04 UTC from IEEE Xplore. Restrictions apply.